RSC Advances

PAPER

View Article Online
View Journal | View Issue

Cite this: *RSC Adv.*, 2025, **15**, 42728

Analysis of tear fluid protein fractions using surface-enhanced Raman spectroscopy (SERS), followed by a high-performance liquid chromatography-light emitting diode-induced fluorescence (HPLC-LED-IF) method

Sphurti. S. Adigal,[a] Sulatha V. Bhandary,[b] Neetha I. R. Kuzhuppilly,[b] Sajan D. George,[c] V. B. Kartha[a] and Santhosh Chidangil *[a]

The present study investigates the application of surface-enhanced Raman spectroscopy (SERS) in conjunction with high-performance liquid chromatography-light-emitting diode-induced fluorescence (HPLC-LED-IF) for analyzing tear proteins in the diagnosis of ophthalmological conditions. SERS is a highly sensitive technique capable of detecting low-concentration biomolecules in body fluids, enabling the monitoring of protein composition, presence, and relative variations associated with different health conditions. In this study, SERS substrates were fabricated by immobilizing gold nanostars on APTES-functionalized surfaces, leveraging the well-known electric field enhancement at sharp plasmonic edges. Tear protein fractions (PF1 and PF2) obtained from the HPLC system were drop-coated onto these substrates for SERS measurements. Tear fluid samples from control (C), moderate dry-eye (MDE), and primary open-angle glaucoma (POAG) subjects were studied, and the recorded SERS spectra revealed distinct Raman spectral patterns for each disease category. Multivariate analysis using principal component analysis (PCA) for PF1 and PF2 from the control and disease groups explained approximately 88% of the cumulative variance, indicating a clear separation between the groups. Further, classification using *K*-nearest neighbours (KNN) with leave-one-out cross-validation (LOOCV) approach for PF1 and PF2 showed 85% sensitivity, 90% specificity, and 88% accuracy, suggesting that this bimodal approach (HPLC-LED-IF + SERS) has the potential to improve the classification of disease states compared to HPLC-LED-IF alone.

Received 30th July 2025
Accepted 23rd October 2025

DOI: 10.1039/d5ra05549k

rsc.li/rsc-advances

1 Introduction

Detection and molecular characterization of biomarkers in body fluids remain challenging owing to their complex and heterogeneous composition.[1–5] Single analytical methods are often inadequate, providing either limited sensitivity for detection or insufficient molecular specificity for structural elucidation. The integration of complementary techniques has therefore become a preferred strategy, enabling the simultaneous detection of target analytes and characterization of their molecular features.[6,7]

Surface-enhanced Raman spectroscopy (SERS) offers high sensitivity and molecular specificity by providing vibrational fingerprints of analytes at trace levels.[8] However, its direct application to body fluids is limited by strong matrix interferences, low reproducibility, and restricted analyte diffusion to active nanometallic surfaces.[9] These limitations compromise both sensitivity and robustness. Despite these drawbacks, SERS has been successfully applied in biofluid analysis, including serum and urine, to differentiate pathological conditions by exploiting subtle spectral variations.

To overcome the intrinsic limitations of SERS, separation techniques have been coupled with vibrational spectroscopy. Approaches such as thin-layer chromatography (TLC)-SERS and phase separation have demonstrated improved analyte discrimination in complex samples.[10–15] Among these, high-performance liquid chromatography (HPLC) remains the most widely used separation method.[9] The feasibility of HPLC-SERS was initially demonstrated by Freeman *et al.* for para-rosaniline hydrochloride, achieving sensitive detection across several orders of magnitude.[16] Since then, HPLC-SERS has been

[a]*Centre of Excellence for Biophotonics, Manipal Institute of Applied Physics, Manipal Academy of Higher Education, Manipal, Karnataka, 576104, India. E-mail: santhosh.cls@manipal.edu*

[b]*Department of Ophthalmology, Kasturba Medical College, Manipal, Manipal Academy of Higher Education, Manipal, Karnataka, 567104, India*

[c]*Centre for Applied Nanosciences, Manipal Institute of Applied Physics, Manipal Academy of Higher Education, Manipal, Karnataka, 567104, India*

successfully applied in diverse contexts, including the quantification of antibiotics in milk, melamine in food products, pesticide residues in fruits, adulterants in dietary supplements, and toxic contaminants in water.[8,10,17–20] In a recent study, Zeng *et al.* used HPLC to purify compounds from sea cucumber culture sediment and then applied SERS to the effluent, achieving a detection limit as low as 1 ng for the target analyte and illustrating effective separation prior to Raman measurement.[17] These works confirm not only the feasibility of HPLC-SERS for trace analyte detection but also its adaptability to complex sample streams. Despite these advances, prior studies have primarily focused on small molecules or complex mixtures in general biofluids, and none have applied HPLC-SERS in combination with LED-induced fluorescence for detailed analysis of protein fractions. This gap underscores the need for a strategy that integrates sensitive protein profiling with molecularly specific Raman characterization, offering both detection and structural insights.

To address this gap, chromatographic separation methods that provide sensitive protein profiling are required. In this regard, our previous studies employed HPLC-LED-IF to record the profiles of tear proteins, providing a robust platform for fractionation and initial detection.[21,22] This method utilises a reverse-phase C8 column for hydrophobic separation and fluorescence detection at an emission wavelength of 340 nm following excitation at 280 nm. The approach demonstrated high sensitivity and specificity, successfully differentiating conditions such as MDE and POAG.[21,22] Nevertheless, fluorescence detection provides only global protein profiling and lacks molecular resolution for characterizing individual protein fractions.

The integration of HPLC-LED-IF with SERS enables detailed molecular characterization of protein fractions that cannot be achieved by fluorescence profiling alone. SERS provides vibrational fingerprints of biomolecules, allowing the detection of subtle structural variations associated with disease.[23,24] By applying SERS to chromatographically separated fractions, it is possible to complement HPLC-LED-IF's protein profiling with molecularly specific information, enhancing both detection and characterization capabilities.

Achieving sensitive and reproducible SERS measurements for protein fractions requires substrates that provide strong and consistent Raman signal enhancement. Nanostructured substrates, particularly gold nanostars, are advantageous due to their sharp tips and high surface curvature, which generate intense localized electromagnetic fields and amplify molecular vibrations.[25–30] Functionalization strategies, such as APTES-mediated nanoparticle immobilization, further ensure uniform analyte adsorption and improve reproducibility.[31–37] In general, DCDRS has been used to concentrate protein fractions at the droplet edge during drying, thereby enhancing both signal intensity and spectral resolution. When combined with SERS, it provides a robust approach for the molecularly specific characterisation of complex protein samples.[38–42] Such approaches demonstrate how Raman-based methods can complement chromatographic separation, enhancing the detection of subtle structural differences in biomolecules.

To leverage the complementary strengths of chromatographic separation and molecularly specific Raman detection, the present study applied an integrated HPLC-LED-IF and SERS approach to tear PF1 and PF2. This approach enabled the identification of subtle spectral differences between fractions, resulting in improved classification of MDE and POAG compared with controls. In addition, multivariate statistical analysis was employed, where PCA was used for cluster analysis and a KNN leave-one-out method was applied to evaluate classification performance in terms of sensitivity, specificity, and accuracy. Recent advances have also highlighted the utility of machine learning-assisted SERS for biomedical applications.[43–45] Lin *et al.* reported a deep-learning-assisted SERS platform capable of ultrasensitive diagnosis of ovarian cancer with high classification accuracy.[46] Xu *et al.* demonstrated machine learning approaches for analyzing complex SERS spectra in cellular systems.[47] Such studies illustrate how data-driven approaches are increasingly enhancing SERS analysis, complementing experimental advances in sensitivity and reproducibility. By combining fluorescence-based profiling with sensitive Raman analysis, the study establishes a novel and robust methodology for comprehensive tear protein fraction characterization, demonstrating both feasibility and potential clinical utility. These findings underscore the promise of this platform as a non-invasive tool for biomarker-based diagnostics in ocular diseases.

2 Experimental section

2.1 Sample collection

Ethical clearance was obtained from the Institutional Ethics Committee, Kasturba Medical College, Manipal (IEC 230/2019) and the Indian Council of Medical Research (ICMR) for sample collection and measurements. Informed consent was obtained from each volunteer prior to participation. Samples from 20 controls, 20 MDE subjects, and 20 POAG patients were collected using Schirmer strips (Table 1). Volunteers were asked to position their heads at a slight angle so that tears were directed toward the lower fornix, thereby avoiding reflex tearing. The lower eyelid of the left eye was gently pulled down, and the tip of the strip was placed in contact with the tear meniscus without irritating the conjunctiva. The strips were observed to be wet by more than 15 mm in all 20C and 20 POAG subjects and 5–10 mm in 20 MDE cases. POAG patients exhibited optic nerve damage, as evidenced by structural changes, including diffuse or focal neuroretinal rim thinning (observed on slit-lamp evaluation with a +90 diopter lens or optical coherence tomography) and/or functional glaucomatous visual field defects on standard automated perimetry, with no secondary

Table 1 Sample details

No. of subjects	Gender	Age	Clinical diagnosis
1–20	13 F, 7 M	>40	C
21–40	10 F, 10 M	>40	MDE
41–60	11 F, 9 M	>40	POAG

causes identified for the damage. Additionally, all POAG patients had open angles on gonioscopy and pretreatment intraocular pressures greater than 21 mmHg. Subjects with renal, hepatic, gastrointestinal, or neurologic disease, ocular surgery, ocular inflammation, diabetic retinopathy, myopia, or glaucoma other than POAG were excluded from the study. Detailed subject information is provided in SI.

Then the strips were placed in Eppendorf tubes (1.5 mL) and immersed in 150 μL of HPLC grade water separately and immediately centrifuged at 503 g (3000 rpm) for 5 minutes, the resulting solutions were stored at \80 °C until analysis. A low centrifugal force was set to minimise the chance of protein loss during centrifugation of the sample. Later, the samples are run in HPLC-LED-IF for protein fraction collection.

2.2 Substrate synthesis

APTES 97%, chloroauric acid trihydrate ($HAuCl_4 \cdot 3H_2O$), silver nitrate ($AgNO_3$), and ascorbic acid (AA) were procured from Merck, while lysozyme (Lyz) was obtained from Sigma-Aldrich. The reagents were used as received without any further purification.

Gold (Au) nanostructures were prepared using the seed-mediated synthesis technique. Initially, seed nanoparticles were synthesised, and a small amount of these seeds was then added to a growth medium containing the necessary precursors, which facilitated the formation of anisotropic nanostructures.[62] The protocol for synthesizing nanostars closely adhered to the procedure described in the recent studies.[48–50]

The synthesis process began by mixing 10 mL of a 250 μM trisodium citrate solution with 10 mL of a 250 μM $HAuCl_4$ solution in a beaker, followed by gentle stirring for 10 minutes. Subsequently, 600 μL of an ice-cold 0.1 M $NaBH_4$ solution was added to the stirring mixture, and stirring continued for an additional 5 minutes. Afterwards, the stirring was stopped, and the solution was carefully cooled to 4 °C. This process resulted in a striking orange-wine-red colour, visually confirming the successful formation of gold nanoseeds. The Au seed particles were measured to be 8 nm in diameter using the particle size analyzer (Horiba Scientific Nano Particle Analyzer SZ-100) with a zeta potential of −65.1 mV.

Then, a 30 μL aqueous solution of 1 M HCl was added to a 10 mL solution with a concentration of 0.25 mM. Subsequently, 300 μL of the seed solution was introduced to the mixture while stirring continuously. Following this, under stirring, 300 μL of a 2 mM $AgNO_3$ solution and 150 μL of a 0.1 M L-ascorbic acid solution were added rapidly. Notably, the solution's color rapidly changed from orange-wine-red to blue. The particle size of the Au nanostars was determined to be 85 nm in diameter using a field-enhanced scanning electron microscope (7610FPLUS, JEOL instrument), and the corresponding zeta potential was −26 mV measured using the nanoparticle analyser.

2.3 Fabrication of SERS-active substrates

2.3.1 Instrumentation. The schematic of the experimental setup for the SERS measurement is shown in Fig. S1 (see in the (SI)), which includes an excitation laser (Torsana, Star Bright, Sweden) with a 785 nm laser line and 500 mW of power. The 785 nm wavelength is chosen to reduce fluorescence interference from the samples. A holographic filter is used to remove unwanted background emissions from the laser by selectively transmitting radiation at 785 nm while blocking other wavelengths. To eliminate Rayleigh scattering and collect the Raman scattered radiation, an edge filter is placed just in front of the spectrometer slit. The optimisation process begins by determining the suitable laser power and selecting the appropriate microscope objective. The laser beam is focused by the microscope objective and directed onto the sample cell.

For sample analysis, protein fractions collected from the HPLC-LED-IF system are placed in the sample cell. The path selector functions as a switch between the CCD camera and spectrometer, allowing for the observation of the sample and data acquisition. Proper beam alignment and focal positioning are achieved using a 1 : 1 ratio telescopic setup with two convex lenses, each having a focal length of 30 cm. A dichroic mirror is used to direct (reflect) the 785 nm beam to the sample and transmit the back-scattered Raman radiation to the spectrometer. A spectrograph combined with a liquid nitrogen-cooled CCD detector (iHR 320, Horiba Jobin Yvon) enabled accurate and sensitive recording of the Raman spectra.

All spectral measurements were conducted using a laser power of 6.2 mW, an acquisition time of 10 seconds, and a 50× objective. To assess the reliability and consistency of the DCD-SERS method, measurements were taken at five multiple spots across the same substrate.

The reproducibility of SERS measurement is highly dependent on the quality of the fabricated substrate. To assess the precision or reproducibility of measurements within this study, the relative standard deviation (RSD) was calculated for the prominent peak at 1664 cm^{-1} in the SERS spectra using the following formula $\text{RSD}\ (\%) = \left(\frac{\text{Standard Deviation}}{\text{Mean}}\right) \times 100\%$.[65] To assess the effectiveness of the employed SERS technique, measurements were conducted to estimate the limit of detection (LOD) using Lyz at various concentrations, focusing on the Raman frequency at 1664 cm^{-1}. The LOD was calculated using the standard formula $\text{LOD} = \frac{3.3 \times \sigma}{\text{Slope}}$, where σ is the standard deviation, and the slope is obtained from the calibration curve of SERS intensity *versus* solute concentration.[21] To verify the substrate's quality, the SERS enhancement factor (EF) was calculated for the prominent band at 1664 cm^{-1} using the formula: $EF = (I_{SERS}/I_{RAMAN}) \times (C_{RAMAN}/C_{SERS})$. This parameter serves as a quantitative measure of signal amplification relative to conventional Raman spectroscopy.

After evaluating the SERS substrate's effectiveness through the calculation of the enhancement factor, the study was extended to the spectral analysis of major tear proteins. These tear components are essential for ocular functionality and serve as crucial defence mechanisms against infectious agents.[51,52] The role of Lyz in tears has been widely recognized, with numerous studies highlighting its antimicrobial activity and

involvement in immune regulation within the ocular environment.[53,54] Lyz has been considered a typical marker for dry eye in various investigations, emphasising its potential significance in ocular health[55,56] Moreover, recent findings underscore the involvement of Lyz in inflammatory processes within the eye in glaucoma conditions.[57,58]

Lyz is typically present in tears at concentrations of a few mg mL^{-1}, making it an ideal candidate for SERS-based analysis. Prior to the SERS investigation, Lyz was identified using the HPLC-LED-IF technique.[21,22] In this analysis, the co-injection method was applied, where a known concentration of Lyz was injected along with the sample to confirm the identity of the protein peak based on co-elution. Through this approach, protein fraction 1 (PF1) was identified as Lyz. To further confirm the spectral identity of Lyz in the SERS analysis, the spiking method was employed. In this approach, a known quantity of Lyz was added to the sample, and the resulting spectral changes were compared with the original spectra. This validation confirmed that the observed SERS features corresponded specifically to Lyz, supporting its reliable detection and characterization in tear samples.

2.3.2 Protein fractions collection. Protein fractions from 20C, 20 MDE, and 20 POAG tear fluid samples were collected using the HPLC-LED-IF system and then stored at −80 °C for further analysis. The fractions of the respective tear fluid samples were collected as part of our previous work, and the details of the sample collection procedure are described elsewhere.[21,22] For the C group, protein fractions from 20 individuals were obtained: protein fraction 1 (PF1) and protein fraction 2 (PF2) were collected at their respective elution times during the same runs. Specifically, at the elution time of 2317 seconds, PF1 was collected, followed by PF2 at the elution time of 2385 seconds in the same chromatographic run. As shown in our earlier studies, these retention times were validated by co-injection with protein standards, confirming PF1 as Lyz and PF2 as lactoferrin (LF).[21,22] These two proteins were selected for further SERS analysis because they are the major tear proteins, exhibit the highest chromatographic intensities, and contribute significantly to the differentiation between C, MDE, and POAG groups in previous statistical analyses. Both fractions were derived from the same set of samples during their respective runs. Fig. 1 illustrates the process of collecting PF1 and PF2 and drop coating them onto the SERS substrate.

A 2 μL droplet from each sample was deposited onto a gold nanoparticle substrate and left to air-dry in a desiccator at room temperature. Using a 50× objective with 0.6 NA, and laser power of 6.2 mW, SERS signals were recorded by focusing the laser beam on the dried droplets with an acquisition time of 10 seconds.

3 Results

3.1 Spectral characterization of plasmonic nanostars

UV-vis spectroscopy is employed to investigate the localized surface plasmon resonance (LSPR) characteristics of plasmonic nanostructures. The gold nanoseed solution exhibits an absorption peak at approximately 515 nm (Fig. S2(a) (see SI)), whereas the gold nanostar solution shows an absorption maximum at 700 nm (Fig. S2(b) (see SI)).

UV absorption of the nanostars attached to the APTES-functionalized substrate was measured on the 1st day of their preparation, revealing a peak at 715 nm (Fig. 2(a)). To evaluate their stability, the UV absorption spectra of the nanostars were monitored over seven consecutive days. Notably, the absorption maximum consistently remained at 715 nm throughout the seven-day period, with minimal shifts in the peak position related to the LSPR (Fig. 2(a)). After three days of substrate preparation, a FESEM image was captured using a FESEM (7610F PLUS, JEOL) instrument, providing detailed visual insight into the morphology of the nanostars on the APTES-functionalized surface (Fig. 2(b)).

3.2 Assessment of reproducibility, limit of detection (LOD) and enhancement factor

Reproducibility measurement evaluated using RSD for the prominent peak at 1664 cm^{-1} with a mean of 352.4 ± 17.8. is indicated by a 5% RSD value in Fig. S3 (see SI). The average of five detection spots (average of 25 spectra) is also presented for clarity Fig. S3(c) (see SI). Fig. 3(a) represents the SERS of Lyz at different concentrations at 10 nM, 100 nM, 1 μM, 10 μM and 100 μM. The resulting LOD is 0.24 nM (Fig. 3(b), showcasing the substrate's capability in measuring tear protein fractions collected from the HPLC-LED-IF system, which can range in concentration from μM to nM.[21,22] In the present study, the enhancement factor corresponding to the intense Raman band at 1664 cm^{-1}, calculated from the measured intensities I_{SERS} = 336 and I_{RAMAN} = 70.83 was estimated to be approximately 4.7

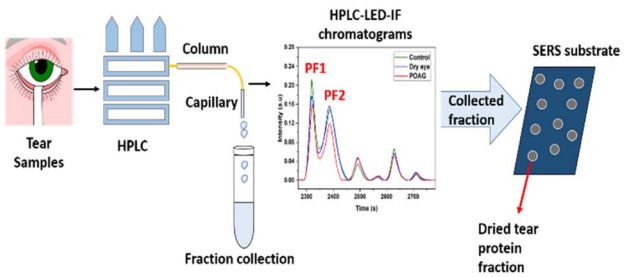

Fig. 1 Illustration of the HPLC-LED-IF process, including the collection of tear protein fractions and the drop coating onto the SERS substrate.

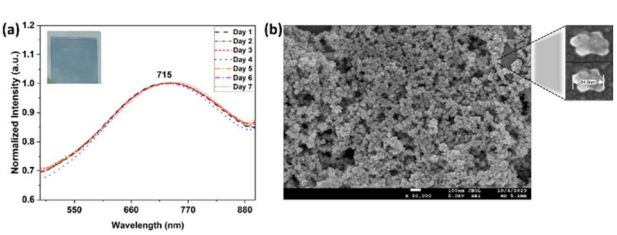

Fig. 2 (a) UV-absorption spectra of APTES-associated gold nanostar substrate on seven different days with a photograph of the fabricated substrate (inset), (b) FESEM image of the nanostar substrate.

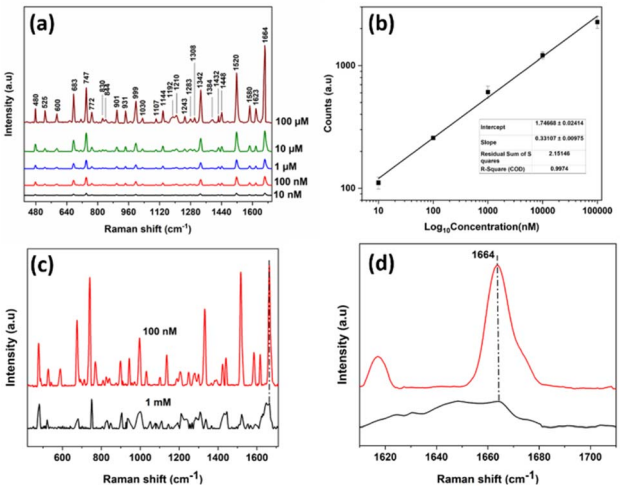

Fig. 3 (a) The SERS of Lyz at different concentrations: (a) 10 nM, 100 nM, 1 μM, 10 μM and 100 μM, (b) corresponding linear fit-plot of Lyz concentrations (10 nM, 100 nM, 1 μM, 10 μM, 100 μM) for the Raman peak at 1664 cm^{-1}, (c) comparative analysis of Raman spectrum of Lyz (1 mM) and SERS spectrum of Lyz (100 nM), and (d) enlarged Raman and SERS spectra of 1 mM and 100 nM Lyz.

$\times 10^6$. This result indicated that the SERS signal for Lyz at 100 nM concentration experiences a 10^6-fold increase in intensity compared to the conventional Raman signal at 1 mM (Fig. 3(c) and (d). The frequency assignments of Raman bands in the Lyz spectra in this study fully match those reported in the available literature, based on DCD-SERS and SERS methodologies, as given in Table 2.[59–64]

3.3 SERS study of the tear fluid fractions PF1 and PF2

The spectra of PF1 and PF2 were recorded and pre-processed for statistical analysis. Pre-processing of Raman spectra aimed to eliminate unexpected and non-significant variations within the spectra, such as spikes, background fluorescence, and fluctuations in signal intensity, to enhance the accuracy and reliability of subsequent data analysis. The software Unscrambler X (version 10.4 CAMO, Norway) was used for the pre-processing.[65] All protein profiles underwent vector normalization. The average SERS spectra of the two protein fractions (PF1 and PF2) from C, MDE, and POAG samples (20 each) were plotted to visualize the spectral patterns in the tear protein fractions Fig. 4(a) and 5(a). A comparison of the spectra belonging to three categories has revealed spectral differences that can distinguish between C, MDE, and POAG conditions. Notably, certain Raman bands (480, 600, 683, 747, 805, 844, 931, 1107, 1135, 1361, 1456, 1580 cm^{-1}) were common across all fractions, while other bands were uniquely present or absent in PF1 and PF2. The corresponding peak assignments are given in Table 3, corroborated by relevant literature.[59,61,66,67] Difference spectra were used to pinpoint significant distinctions in MDE and POAG compared to the C. Fig. 4(b) illustrates the differences in the entire spectra of tear fluid fraction PF1 of MDE and POAG compared to the C PF1. It is evident that the "MDE" and "POAG"

Table 2 Assignment of SERS (from gold nanostar substrate) signals of Lyz[a,59–64]

Raman shifts (SERS) in cm^{-1}	Assignment/molecular groups
480	—
525	SS bridge str
600	Phe
683	—
747	Trp
772	Trp: δ (CH)
830	Tyr doublet
844	$\nu(C_\alpha\text{-N}, C\text{–}C)$, Tyr
901	N–C_α–C stretching
931	ν(N–C_α–C)
999	Phe (ring breathing of benzene)
1030	Phe
1107	Trp
1144	ν(C–N)
1192	Tyr + Phe
1210	Tyr
1243	Amide III
1283	Amide III
1308	—
1342	Trp
1384	COO^- symm. str
1432	δ (CH_2)
1448	Amide II + His (CH2 scissoring)
1520	—
1580	Histidine (C═C str.)
1623	Trp + Phe
1664	Amide I

[a] Abbreviations: ν-stretching, δ-deformation co-ordinate, symm.-symmetric, str.-stretching, Tyr-tyrosine, Trp-tryptophan, Phe-phenylalanine, His-histidine.

samples not only differ from the C but also differ from each other. Similarly, Fig. 5(b) shows the differences in SERS bands of PF2 in MDE and POAG compared to C PF2.

4 Data analysis

4.1 Tear fluid fractions analysis

This section discusses the PCA of SERS spectra of the tear fluid fractions PF1 and PF2 using the Unscrambler X software

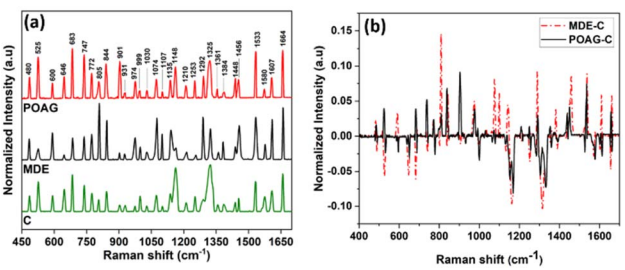

Fig. 4 (a) Average SERS spectra (20 each) of the tear fluid PF1 fractions of three types of samples (C, MDE, and POAG conditions) in the region 450–1700 cm^{-1} and (b) difference spectra of PF1 of the mean of MDE and mean of POAG samples.

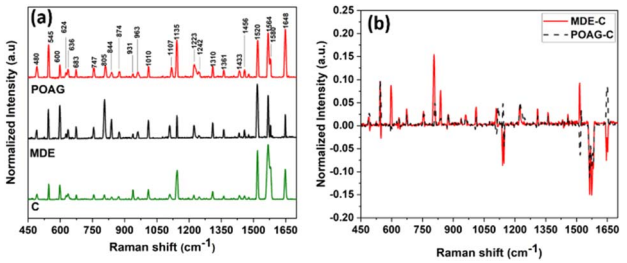

Fig. 5 (a) Average SERS spectra (20 each) of the tear fluid fractions PF2 of three types of samples (C, MDE, and POAG conditions) in the region 450–1700 cm^{-1} and (b) difference spectra of PF2 of the mean of MDE and the mean of POAG samples.

(version 10.4, CAMO, Norway).[65] The initial analysis examined the entire Raman spectral range to identify differences in Raman shifts among C, MDE and POAG tear protein fractions. The PCA, performed across the entire spectrum, revealed notable variations, particularly in PC1 and PC2 when comparing MDE and POAG with the C. While the difference spectra highlighted variations in Raman bands, the factor loadings represented by PC1 and PC2 elucidated the contributions of specific Raman bands to the observed differences.

In Fig. 6(a) and (b), the PC1 *versus* PC2 score plot with corresponding factor loadings shows the variations captured by the principal components. As typically observed, PC1 contributes more to the variance than the subsequent principal components. In this analysis, the cumulative percent variance reached 88% due to the contributions of the PC1 and PC2 components. The PCA results demonstrated precise classification for distinguishing MDE and POAG from the C when analyzing the entire SERS spectra of PF1, spanning from 450 cm^{-1} to 1700 cm^{-1}. In Fig. 7(a) and (b), the PC1 *versus* PC2 score plot with corresponding factor loadings illustrates the classification of C, MDE, and POAG conditions obtained from the PCA.

Additionally, the factor loading plots indicated that specific SERS bands in PF1 and PF2 contributed significantly to the observed spectral variations. For PF1, the major contributors in PC1 were bands at 600 cm^{-1}, 805 cm^{-1}, 1148 cm^{-1} (ν(C–N)), 1292 cm^{-1} (Amide III), and 1456 cm^{-1} (δ (CH_2)), while in PC2 the peaks at 901 cm^{-1} (N–C_α–C stretching), 1325 cm^{-1} (Phe + His), and 1533 cm^{-1} (C–C stretching) were most relevant. In PF2, the peaks with higher loadings in PC1 included 805 cm^{-1}, 1135 cm^{-1} (ν(C–N)), 1520 cm^{-1} (δ (NH_3^+)), and 1580 cm^{-1} (His C–C stretching), whereas in PC2 the peaks at 545 cm^{-1} (C–COO^- asymmetric bending, Trp), 1520 cm^{-1} (δ (NH_3^+)), 1564 cm^{-1} (NH_2 scissoring), and 1648 cm^{-1} (Amide I) showed significant contributions.

To further evaluate diagnostic performance, we performed a KNN analysis with LOOCV for PF1 ($K = 3$) and PF2 ($K = 3$). The following metrics were calculated using standard formulas for each class:[21,22]

$$\text{Sensitivity(True positive rate(TP))} = \frac{\text{TP}}{\text{TP} + \text{FN}}$$

$$\text{Specificity(True negative rate(TN))} = \frac{\text{TN}}{\text{TN} + \text{FP}}$$

$$\text{Precision(Positive predictive value)} = \frac{\text{TP}}{\text{TP} + \text{FP}}$$

$$\text{Accuracy} = \frac{\text{TP} + \text{TN}}{\text{TP} + \text{TN} + \text{FP} + \text{FN}}$$

Table 3 Assignment of SERS spectra of PF1 and PF2 based on available literature[a] [59,61,66,67]

Raman shifts of protein fractions(cm^{-1})		Raman band assignment/molecular groups
PF1	PF2	
480	480	—
525	—	SS bridge str
—	545	C–COO^- asymmetric bend (Trp)
600	600	Phe
—	624	Phe
—	636	Tyr: δ (R, CH), ν(C–S)
646	—	Tyr
683	683	δ (C–H), δ (R), δ (COO^-)
747	747	Trp
772	—	Trp: br (indole) symm, δ (CH)
805	805	—
844	844	ν(C_α–N, C–C), Tyr
—	874	N–H bend
901	—	N–C_α–C str
931	931	ν(C_a–C–N)
—	963	ν(C–C)
974	—	Tyr
999	—	Phe (ring breathing of benzene)
—	1010	Phe + Tyr
1030	—	Phe
1074	—	ν(C–N)
1107	1107	Trp
1135	1135	ν(C–N)
1148	—	ν(C–N)
1210	—	Tyr
—	1223	—
—	1242	Amide III
1253	—	AmideIII
1292	—	Amide III, δ (CH_2, CH_3), CH bend
1310	1310	—
1325	—	Phe + His
1361	1361	Trp
1384	—	COO^- symmetric str
—	1433	δ (CH_2)
1448	—	Amide II + histidine (CH_2 scissoring)
1456	1456	δ (CH_2)
—	1520	δ (NH_3^+)
1533	—	C–C str
—	1564	NH_2 scissors
1580	1580	Histidine (C=C stretching)
1607	—	Tyr
—	1648	Amide I
1664	—	Amide I

[a] Abbreviations: R – benzene ring, wag-wagging, Glu-glutamic acid.

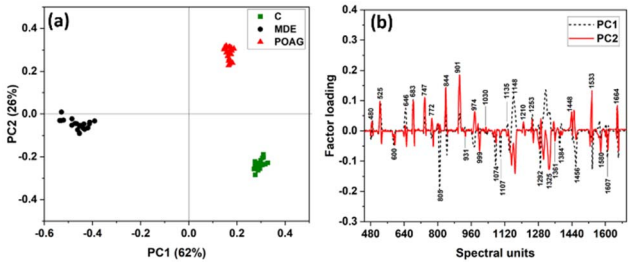

Fig. 6 (a) PC1 *vs.* PC2 score plot obtained for the SERS spectra of C, MDE, and POAG for PF1 and (b) corresponding factor loading plots for PC1 and PC2.

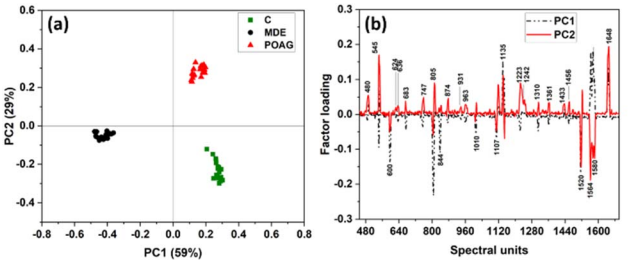

Fig. 7 (a) PC1 *vs.* PC2 score plot obtained for the SERS spectra of C, (b) MDE and (c) POAG protein for PF2 and (b) corresponding factor loading plots for PC1 and PC2.

Table S1 (see SI) describes the multi-confusion matrix (TP, misclassified), indicating for the PF1 column summarises the number of TP for each class along with the misclassified sample. For class C, 18 samples were correctly classified as C (TP), while 1 sample were misclassified as MDE and 1 as POAG. Similarly, for MDE, 18 samples were correctly classified, with 1 misclassified as C and 1 as POAG. For POAG, 17 samples were correctly classified, with 3 misclassified as MDE and none as C. Table S2 (see SI) summarizes the number of TP for each class, along with the misclassified samples indicating for PF2. For class C, 17 samples were correctly classified as C (TP), while 2 samples were misclassified as MDE and 1 as POAG. Similarly, for MDE, 16 samples were correctly classified, with 3 misclassified as C and 1 as POAG. For POAG, 16 samples were correctly classified, with 1 misclassified as C and 3 as MDE.

The classification performance of the KNN model using LOO-CV is depicted as in Fig. S4 (see SI). Fig. S4(a) displays the misclassification curve, where green points represent correctly classified samples and red points indicate misclassifications. Fig. S4(b) compares true *versus* predicted classes (C, MDE, and POAG), showing that C samples are classified with high accuracy, MDE samples are generally predicted correctly with some confusion toward POAG, and POAG samples exhibit the highest rate of misclassification. Fig. S5 illustrates the same evaluation for another dataset/feature set. In subplot Fig. S5(a), most samples again fall under correct classification with some scattered misclassifications. Subplot Fig. S5(b) highlights the class-wise predictions, where C samples are consistently well-identified, MDE samples show reasonable accuracy but

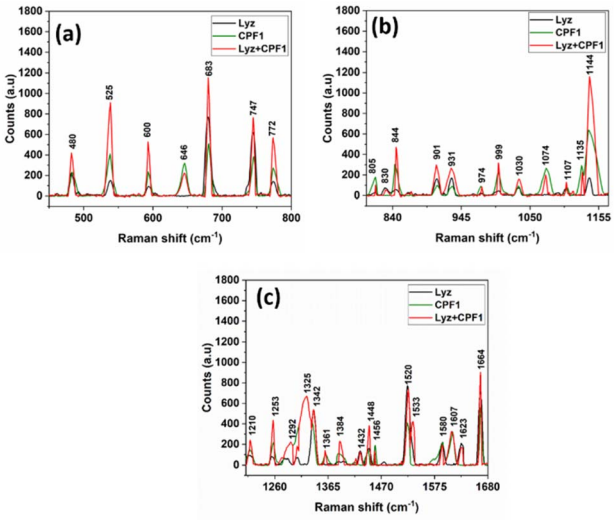

Fig. 8 SERS spectra of Lyz, C PF1 and Lyz + C PF1 at 10 s, 6.2 mW power in region (a) 450–800 cm^{-1}, (b) 800–1170 cm^{-1} and (c) 1200–1680 cm^{-1}.

occasional misclassification, and POAG samples remain the most challenging, with a larger proportion predicted incorrectly.

Overall, across both figures, the KNN model demonstrates a strong ability to distinguish Control subjects but struggles to clearly separate MDE from POAG, reflecting overlapping characteristics between these groups.

4.2 Spiking-based verification of PF1

The spiking study revealed that the introduction of 100 nM Lyz into C tear protein fraction 1(Lyz + C PF1) resulted in an increased intensity of several SERS bands (480, 525, 600, 683, 747, 772, 844, 901, 931, 999, 1030, 1074, 1144, 1210, 1253, 1384, 1448, 1580 and 1664 cm^{-1}) (Fig. 8), exactly overlapping with standard Lyz bands (Fig. 6) and thereby confirming the presence of Lyz. The bands at 646, 805, 1074, 1135, and 1456 cm^{-1} did not show a similar enhancement. A comprehensive analysis of the SERS peak intensity changes resulting from the Lyz spiking effect on the Raman bands of C PF1 is presented in Table 4.

5 Discussion

In this study, UV absorption spectra, showing a shift from 700 nm in solution to 715 nm on the APTES-functionalized substrate, indicated the successful attachment of gold nanostars. The position and shape of the plasmon absorption of silica-gold nanoparticles are influenced by particle size, the surrounding dielectric medium, and surface-adsorbed species. The observed spectral shift and broadening can primarily be attributed to variations in the extinction cross-section, and the electron mean free path within the metal shell.[68,69]

The 5% RSD and 0.24 nM LOD demonstrated the high reproducibility and sensitivity of a SERS substrate for detecting

Table 4 Raman band intensity variations in the CPF1 spectrum after Lyz spiking

Lyz (present study) (cm^{-1})	CPF1 (cm^{-1})	Lyz + CPF1	Raman band assignment/molecular groups
480	480	↑	—
525	525	↑	SS bridge
600	600	↑	Phe
683	683	↑	—
747	747	↑	Trp
772	772	↑	Arginine
844	844	↑	Tyr
901	901	↑	N–C_α–C stretching
931	931	↑	ν(Ca–C–N)
999	999	↑	Phe (ring breathing)
1030	1030	↑	Phe
1107	1107	↑	Trp
1210	1210	↑	Tyr/Phe
1253	1253	↑	Amide III β-sheet
1384	1384	↑	COO^- symmetric stretch
1448	1448	↑	Amide II + histidine
1580	1580	↑	Histidine (C=C stretching)
1664	1664	↑	Amide I

and analyzing low-concentration protein fractions in body fluids. Additionally, a 10^6-fold enhancement in SERS signal intensity for Lyz at 100 nM compared to the conventional Raman signal at 1 mM underscored the substrate's effectiveness in detecting low-concentration protein fractions, highlighting its potential for sensitive and precise analysis of body fluid samples in biomedical applications. The stable attachment of gold nanostars on APTES-functionalized substrates ensures uniform analyte adsorption, which is critical for reproducible SERS measurements. The anisotropic morphology of nanostars, with sharp tips and high curvature, generates strong electromagnetic enhancement at localized surface plasmon resonance (LSPR) sites, further improving Raman signal sensitivity.[23,24,31,70,71]

Protein profiling of clinical samples has a crucial role in the development of reliable diagnostic methods for identifying potential protein markers. Our previous studies have underscored the significance of protein profiling in the context of MDE and POAG.[21,22] Similarly, studying the protein profiles of tear fluid fractions holds diagnostic potential, and the adoption of SERS emerges as a valuable tool for detecting biochemical differences. To the best of our knowledge, no previous studies have applied this combined HPLC-LED-IF and SERS approach to tear protein fractions. Most prior work has focused on SERS of whole tears, where complex mixtures and high background signals can obscure individual protein contributions. Meanwhile, HPLC allows the initial separation and collection of individual protein fractions, significantly reducing sample complexity. Applying SERS to these isolated fractions enhances spectral signals and minimises background interference, enabling more precise and specific characterisation of protein profiles.

Building on this novelty, it is noteworthy that while some studies have analyzed whole tear fluid using SERS, these investigations are limited in scope and do not focus on fractionated protein analysis. This is the first study to report the application of gold nanoparticle (nanostar) substrates for analyzing tear protein fractions. Moreover, this work demonstrates the advantages of focusing on protein fractions for understanding biochemical variations related to ocular disease.

In this study, only two protein fractions PF1 and PF2 were selected for analysis, as they exhibited the highest chromatographic intensities and showed the most significant contributions to group differentiation (C, MDE and POAG) based on statistical analysis.[21,22] In the present study, the spectral differences observed in the tear PF1 and PF2 of C, MDE and POAG indicated that the spectral patterns are sensitive to the associated health conditions, making them valuable for diagnostic purposes. Using PCA, we examined the entire Raman spectral range to identify significant differences among C, MDE, and POAG tear protein fractions. The PCA results, particularly the contributions of PC1 and PC2, revealed clear classification capabilities, with an 88% cumulative variance explained. This high level of variance capture demonstrates the robustness of the analysis in distinguishing between different tear protein profiles. Notably, certain SERS bands in PF1 and PF2 made significant contributions to the observed variations. For PF1, bands at 805 cm^{-1}, 901 cm^{-1}, 1148 cm^{-1}, 1292 cm^{-1}, 1325 cm^{-1}, and 1533 cm^{-1} were key influencers, while for PF2, bands at 545 cm^{-1}, 805 cm^{-1}, 1520 cm^{-1}, 1564 cm^{-1}, 1580 cm^{-1}, and 1648 cm^{-1} played significant roles. These findings underscore the specificity of Raman bands in reflecting the biochemical differences associated with MDE and POAG conditions. KNN with leave-one-out cross-validation (LOOCV) confirmed that SERS, following HPLC-LED-IF fractionation, provides reliable diagnostic performance (85% sensitivity, 90% specificity, and 88% accuracy), although validation with a larger sample set is required. Employing a spiking method has proven the presence of Lyz in CPF1, as identified using the co-injection method by HPLC-LED-IF method. The detail of the co-injection method is described elsewhere.[21,22] This study laid the groundwork for future research, demonstrating the potential of HPLC-LED-IF coupled with SERS to advance ocular health diagnostics.

By combining HPLC-LED-IF with SERS, we achieved a refined and targeted analysis of tear proteins, focusing on distinct protein fractions rather than the entire mixture. This approach improves detection sensitivity and specificity, demonstrating significant classification capabilities among C, MDE, and POAG samples. Multivariate analysis further improved diagnostic accuracy by highlighting the specific Raman bands responsible for differences among groups. Additionally, the LED-based HPLC-LED-IF system ensures stable and reliable fluorescence detection with low-intensity excitation, preventing sample degradation while maintaining sensitivity. The low cost, compact design, and energy efficiency of LED detection further enhance the practicality of this platform for routine biomedical applications.[72]

Overall, this study establishes a methodologically sound and novel approach for analyzing tear protein fractions using HPLC-LED-IF combined with SERS. While the current study focused

on demonstrating feasibility and classification capability, larger sample sizes and complementary techniques will be needed in the future to explore disease-specific mechanisms and medication effects in more detail. In future studies, we plan to perform a comprehensive identification and quantification of tear protein fractions using orthogonal methods such as ELISA, SDS-PAGE, and LC-MS/MS to further characterize these fractions with a larger sample size. Nonetheless, the results provide compelling evidence that SERS analysis of HPLC-isolated protein fractions is feasible, reproducible, and capable of revealing clinically relevant differences, laying a foundation for future studies in ocular diagnostics.

6 Conclusion

This study demonstrates the application of the HPLC-LED-IF method combined with DCD-SERS for the analysis of tear fluid samples in the context of MDE and POAG. Key procedures of DCD-SERS include the synthesis of gold nanostars, the functionalization of substrates with APTES, and the evaluation of substrate quality. The experiments highlighted the importance of laser wavelength, power, and substrate quality, supporting the method's suitability for tear protein analysis. The observed RSD of ~5% indicates good reproducibility of the SERS measurements under the experimental conditions used. At the same time, the LOD study and enhancement factor underscore the efficiency of the substrates and the value of SERS in examining tear protein fractions. Analysis using SERS, combined with PCA and KNN supervised modelling, indicates the feasibility of classifying samples, suggesting that the observed intensity variations of PF1 and PF2 in MDE and POAG may reflect biochemical changes associated with the disease. Overall, the combination of HPLC-LED-IF and SERS shows potential improvement as a rapid and cost-effective approach for monitoring disease-related biochemical changes. Future studies will focus on larger sample sizes by incorporating supervised modelling and carrying out additional detection methods to validate the diagnostic potential and explore its applications to other body fluids for disease detection.

Author contributions

Sphurti S Adigal: methodology, validation, data collection, formal analysis, statistical analysis, writing – original draft; Sulatha V Bhandary: providing samples and reviewing the manuscript; Neetha IR Kuzhuppilly: involved in providing samples for the study; Sajan D George: involved in reviewing the manuscript; Vasudevan Baskaran Kartha: involved in manuscript review and editing; Santhosh Chidangil: conceptualized, supervised, reviewed and edited the manuscript.

Conflicts of interest

The authors declare that they are not involved with any organisation or entity that has a financial interest or conflict of interest.

Data availability

Data will be made available from the corresponding author on request.

Supplementary information: the details of the subjects, Experimental section and the results. See DOI: **https://doi.org/10.1039/d5ra05549k**.

Acknowledgements

The authors are thankful to the Manipal Academy of Higher Education for the experimental facilities. The authors acknowledge the DST-FIST, Government of India, for the wet lab facility, the DBT, Government of India, for the Micro-Raman spectrometer used for SERS measurements, and the VGST, Government of Karnataka, for the HPLC system. Sphurti S Adigal is thankful to Dr TMA Pai Scholarship for the PhD programme, Manipal Academy of Higher Education. The authors are also grateful to the Department of Ophthalmology, Kasturba Medical College, Manipal, Manipal Academy of Higher Education, Manipal, for their support in this study.

References

1 S. Oh, M. Ji, D. Y. Kim, S. Choi, Y. Kee, S. Woo, H. S. Lee, B. Choi, H. J. Park, H. N. Lee and M. J. Paik, Metabolomic Analysis of Amino Acid and Organic Acid Profiles in Tissue From Ovarian Cancer Patients Using High-Performance Liquid Chromatography-Tandem Mass Spectrometry (HPLC-MS/MS) and Gas Chromatography-Tandem Mass Spectrometry (GC-MS/MS), *Anal. Lett.*, 2025, **58**(4), 623–638.

2 P. Amini and J. O. Okeme, Tear Fluid as a Matrix for Biomonitoring Environmental and Chemical Exposures, *Curr. Environ. Health Rep.*, 2024, **11**(3), 340–355.

3 H. Félix-Rivera and S. P. Hernández-Rivera, Raman spectroscopy techniques for the detection of biological samples in suspensions and as aerosol particles: a review, *Sens. Imag. Int. J.*, 2012, **13**(1), 1–25.

4 J. Korram, A. C. Anbalagan, A. Banerjee and S. N. Sawant, Bio-conjugated carbon dots for the bimodal detection of prostate cancer biomarkers *via* sandwich fluorescence and electrochemical immunoassays, *J. Mater. Chem. B*, 2024, **12**(3), 742–751.

5 C. J. Chen, D. Y. Lee, J. Yu, Y. N. Lin and T. M. Lin, Recent advances in LC-MS-based metabolomics for clinical biomarker discovery, *Mass Spectrom. Rev.*, 2023, **42**(6), 2349–2378.

6 I. H. Cho, P. Bhandari, P. Patel and J. Irudayaraj, Membrane filter-assisted surface enhanced Raman spectroscopy for the rapid detection of E. coli O157: H7 in ground beef, *Biosens. Bioelectron.*, 2015, **64**, 171–176.

7 H. Li, Q. xia Zhu, T. sian Chwee, L. Wu, Y. feng Chai, F. Lu and Y. fang Yuan, Detection of structurally similar adulterants in botanical dietary supplements by thin-layer chromatography and surface enhanced Raman spectroscopy combined with two-dimensional correlation spectroscopy, *Anal. Chim. Acta*, 2015, **883**, 22–31.

8 M. Ukaegbu, N. Enwerem, O. Bakare, V. Sam, W. Southerland, A. Vivoni and C. Hosten, Probing the adsorption and orientation of 2, 3-dichloro-5, 8-dimethoxy-1, 4-naphthoquinone on gold nano-rods: a SERS and XPS study, *J. Mol. Struct.*, 2016, **1114**, 197–205.

9 Y. Zhang, S. Zhao, J. Zheng and L. He, Surface-enhanced Raman spectroscopy (SERS) combined techniques for high-performance detection and characterization, *Trends Anal. Chem.*, 2017, **90**, 1–3.

10 A. Y. Khrushchev, E. R. Akmaev, I. V. Kis, A. Y. Gulyaeva and V. O. Bondarenko, Combination of HPLC and SERS detection applied to the analysis of the trace content of amoxicillin in milk, *Vib. Spectrosc.*, 2022, **123**, 103473.

11 W. A. Hassanain, E. L. Izake, A. Sivanesan and G. A. Ayoko, Towards interference free HPLC-SERS for the trace analysis of drug metabolites in biological fluids, *J. Pharm. Anal.*, 2017, **136**, 38–43.

12 E. De Luca, M. Redaelli, C. Zaffino and S. Bruni, A SERS and HPLC study of traditional dyes from native Chinese plants, *Vib. Spectrosc.*, 2018, **95**, 62–67.

13 B. Zeng, Y. Huang and M. Fan, Interference free HPLC-SERS for the trace analysis of residual furazolidones in the aquaculture sediment, *Chemosensors*, 2022, **10**(12), 508.

14 G. Trachta, B. Schwarze, B. Sägmüller, G. Brehm and S. Schneider, Combination of high-performance liquid chromatography and SERS detection applied to the analysis of drugs in human blood and urine, *J. Mol. Struct.*, 2004, **693**(1–3), 175–185.

15 A. Bosi, G. Peruzzi, A. Ciccola, I. Serafini, F. Vincenti, C. Montesano, P. Postorino, M. Sergi, G. Favero and R. Curini, New advances in dye analyses: *in situ* gel-supported liquid extraction from paint layers and textiles for SERS and HPLC-MS/MS identification, *Molecules*, 2023, **28**(14), 5290.

16 R. D. Freeman, R. M. Hammaker, C. E. Meloan and W. G. Fateley, A detector for liquid chromatography and flow injection analysis using surface-enhanced Raman spectroscopy, *Appl. Spectrosc.*, 1988, **42**(3), 456–460.

17 W. Wang, M. Xu, Q. Guo, Y. Yuan, R. Gu and J. Yao, Rapid separation and on-line detection by coupling high performance liquid chromatography with surface-enhanced Raman spectroscopy, *RSC Adv.*, 2015, **5**(59), 47640–47646.

18 K. Shen, Y. Yuan, C. Zhang and J. Yao, Construction of a HPLC-SERS hyphenated system for continuous separation and detection based on paper substrates, *Analyst*, 2022, **147**(18), 4073–4081.

19 D. Y. Lin, C. Y. Yu, C. A. Ku and C. K. Chung, Design, fabrication, and applications of SERS substrates for food safety detection, *Micromachines*, 2023, **14**(7), 1343.

20 M. Lin, L. He, J. Awika, L. Yang, D. R. Ledoux, H. A. Li and A. Mustapha, Detection of melamine in gluten, chicken feed, and processed foods using surface enhanced Raman spectroscopy and HPLC, *J. Food Sci.*, 2008, **73**(8), T129–T134.

21 S. S. Adigal, S. V. Bhandary, N. Hegde, V. R. NidheesH, R. V. John, A. Rizvi, S. D. George, V. B. Kartha and S. Chidangil, Protein profile analysis of tear fluid with hyphenated HPLC-UV LED-induced fluorescence detection for the diagnosis of dry eye syndrome, *RSC Adv.*, 2023, **13**(32), 22559–22568.

22 S. S. Adigal, N. I. Kuzhuppilly, N. Hegde, N. VR, A. Rizvi, R. V. John, S. D. George, V. B. Kartha, S. V. Bhandary and S. Chidangil, HPLC-LED-Induced Fluorescence Analysis of Tear Fluids: An Objective Method for Primary Open Angle Glaucoma Diagnosis, *Curr. Eye Res.*, 2024, **49**(3), 260–269.

23 R. Goel, S. Chakraborty, V. Awasthi, V. Bhardwaj and S. K. Dubey, Exploring the various aspects of Surface enhanced Raman spectroscopy (SERS) with focus on the recent progress: SERS-active substrate, SERS-instrumentation, SERS-application, *Sens. Actuators, A*, 2024, 115555.

24 D. Cialla-May, A. Bonifacio, T. Bocklitz, A. Markin, N. Markina, S. Fornasaro, A. Dwivedi, T. Dib, E. Farnesi, C. Liu and A. Ghosh, Biomedical SERS–the current state and future trends, *Chem. Soc. Rev.*, 2024, **53**, 8957–8979.

25 M. Li, S. K. Cushing, J. Zhang, J. Lankford, Z. P. Aguilar, D. Ma and N. Wu, Shape-dependent surface-enhanced Raman scattering in gold–Raman-probe–silica sandwiched nanoparticles for biocompatible applications, *Nanotechnology*, 2012, **23**(11), 115501.

26 Y. Pei, Z. Wang, S. Zong and Y. Cui, Highly sensitive SERS-based immunoassay with simultaneous utilization of self-assembled substrates of gold nanostars and aggregates of gold nanostars, *J. Mater. Chem. B*, 2013, **1**(32), 3992–3998.

27 F. Eker, E. Akdaşçi, H. Duman, M. Bechelany and S. Karav, Gold Nanoparticles in Nanomedicine: Unique Properties and Therapeutic Potential, *Nanomaterials*, 2024, **14**(22), 1854.

28 R. D. Norton, A. J. Haes and A. V. Tivanski, Effects of Cosolvent on the Intermolecular Interactions between an Analyte and a Gold Nanostar Surface Studied Using SERS, *J. Phys. Chem. C*, 2024, **128**(41), 17543–17551.

29 Z. Xi, R. Zhang, F. Kiessling, T. Lammers and R. M. Pallares, Role of surface curvature in gold nanostar properties and applications, *ACS Biomater. Sci. Eng.*, 2023, **10**(1), 38–50.

30 A. Tukova, N. T. Nguyen, A. Garcia-Bennett, A. Rodger and Y. Wang, Plasmonic nanostars: Unique properties that distinguish them from spherical nanoparticles from a biosensing perspective, *Adv. Opt. Mater.*, 2024, **12**(28), 2401183.

31 M. Y. Kalashgrani, S. M. Mousavi, M. H. Akmal, A. Gholami, N. Omidifar, W. H. Chiang, R. H. Althomali, C. W. Lai and M. M. Rahman, Gold fluorescence nanoparticles for enhanced SERS detection in biomedical sensor applications: current trends and future directions, *Chem. Rec.*, 2024, e202300303.

32 M. E. Khosroshahi, R. Chabok, N. Chung and Y. Patel, Optimization of immersion direction and time of covalently self-assembled monolayer gold nanourchins on glass as SERS substrate, *J. Nanoparticle Res.*, 2023, **25**(5), 97.

33 T. Yaseen, H. Pu and D. W. Sun, Functionalization techniques for improving SERS substrates and their applications in food safety evaluation: A review of recent research trends, *Trends Food Sci. Technol.*, 2018, **72**, 162–174.

34 Q. Su, X. Ma, J. Dong, C. Jiang and W. Qian, A reproducible SERS substrate based on electrostatically assisted APTES-functionalized surface-assembly of gold nanostars, *ACS Appl. Mater. Interfaces*, 2011, **3**(6), 1873–1879.

35 R. Monaghan, in. *Development of Biofunctional and Biocompatible Surfaces for Biodiagnostic Applications Utilising Plasma Enhanced Chemical Vapour Deposition, Doctoral Dissertation*, Dublin City University, 2015.

36 B. Bassi, B. AlbinI, A. D'Agostino, G. Dacarro, P. Pallavicini, P. Galinetto and A. Taglietti, Robust, reproducible, recyclable SERS substrates: Monolayers of gold nanostars grafted on glass and coated with a thin silica layer, *Nanotechnology*, 2018, **30**(2), 025302.

37 M. Mcoyi, K. Mpofu, M. Lugongolo, C. Williamson, S. Ombinda, P. Lemboumba and M. Kufa, Evaluation of nanoparticle fabrication for improved localized surface plasmon resonance response, in. *MATEC Web of Conferences 2024*, EDP Sciences, vol. **406**, p. 10002, DOI: 10.1051/matecconf/202440610002.

38 K. M. Thomas, S. Ajithaprasad, N. M, M. S Pavithran, S. Chidangil and J. Lukose, Raman spectroscopy assisted tear analysis: A label free, optical approach for noninvasive disease diagnostics, *Exp. Eye Res.*, 2024, **243**, 109913.

39 Z. Guo, M. Ma, S. Lu, Y. Ma, Y. Yu and Q. Guo, Applications of Raman spectroscopy in ocular biofluid detection, *Front. Chem.*, 2024, **12**, 1407754.

40 N. Sunil and B. Pullithadathil, Noninvasive biomarker sensors using surface-enhanced Raman spectroscopy, in. *Nanomaterials for Sensing and Optoelectronic Applications*, 2022, pp. 221–244, DOI: 10.1016/B978-0-12-824008-3.00002-3.

41 J. Park, A. Estrada, K. Sharp, K. Sang, J. A. Schwartz, D. K. Smith, C. Coleman, J. D. Payne, B. A. Korgel, A. K. Dunn and J. W. Tunnell, Two-photon-induced photoluminescence imaging of tumors using near-infrared excited gold nanoshells, *Opt. Express*, 2008, **16**(3), 1590–1599.

42 M. K. Otoufi, N. Shahtahmasebi, A. Kompany, E. K. Goharshadi and A. Roghani, Gradual Growth of Gold Nanoseeds on Silica for Silica@ Gold Core–Shell Nano Applications by Two Different Methods: A Comparison on Structural Properties, *J. Cluster Sci.*, 2014, **25**, 1307–1317.

43 P. P. Kumar, S. Saxena and R. Joshi, Advancements in SERS: Revolutionizing Biomedical Analysis and Applications, *Nanotheranostics*, 2025, **9**(3), 216.

44 G. Fang, X. Lin, X. Liang, J. Wu, W. Xu, W. Hasi and B. Dong, Machine learning-driven 3D plasmonic cavity-in-cavity surface-enhanced Raman scattering platform with triple synergistic enhancement toward label-free detection of antibiotics in milk, *Small*, 2022, **18**(45), 2204588.

45 X. Bi, X. Ai, Z. Wu, L. L. Lin, Z. Chen and J. Ye, Artificial intelligence-powered surface-enhanced Raman spectroscopy for biomedical applications, *Anal. Chem.*, 2025, **97**(13), 6826–6846.

46 S. Lin, M. Dong, C. Li, X. Lin, Y. Cong, W. Xu, Z. Bao and B. Dong, Machine Learning-assisted Ultrasensitive SERS Immunoassays Across Wide Concentration Ranges Toward Clinical Ovarian Cancer Diagnosis, *Adv. Funct. Mater.*, 2025, e09813.

47 J. Wang, L. Cong, W. Shi, W. Xu and S. Xu, Single-cell analysis and classification according to multiplexed proteins *via* microdroplet-based self-driven magnetic surface-enhanced Raman spectroscopy platforms assisted with machine learning algorithms, *Anal. Chem.*, 2023, **95**(29), 11019–11027.

48 H. Yuan, C. G. Khoury, H. Hwang, C. M. Wilson, G. A. Grant and T. Vo-Dinh, Gold nanostars: surfactant-free synthesis, 3D modelling, and two-photon photoluminescence imaging, *Nanotechnology*, 2012, **23**(7), 075102.

49 B. Khlebtsov, E. Panfilova, V. Khanadeev and N. Khlebtsov, Improved size-tunable synthesis and SERS properties of Au nanostars, *J. Nanoparticle Res.*, 2014, **16**, 1–2.

50 N. Schwenk, B. Mizaikoff, S. Cárdenas and Á. I. López-Lorente, Gold-nanostar-based SERS substrates for studying protein aggregation processes, *Analyst*, 2018, **143**(21), 5103–5111.

51 S. Hagan, E. Martin and A. Enríquez-de-Salamanca, Tear fluid biomarkers in ocular and systemic disease: potential use for predictive, preventive and personalised medicine, *EPMA J.*, 2016, **7**, 1–20.

52 P. Ferraboschi, S. Ciceri and P. Grisenti, Applications of lysozyme, an innate immune defense factor, as an alternative antibiotic, *Antibiotics*, 2021, **10**(12), 1534.

53 D. R. Pur, S. H. Krance, A. Pucchio, R. N. Miranda and T. Felfeli, Current uses of artificial intelligence in the analysis of biofluid markers involved in corneal and ocular surface diseases: a systematic review, *Eye*, 2023, **37**(10), 2007–2019.

54 A. Dammak, C. Pastrana, A. Martin-Gil, C. Carpena-Torres, A. Peral Cerda, M. Simovart, P. Alarma, F. Huete-Toral and G. Carracedo, Oxidative stress in the anterior ocular diseases: diagnostic and treatment, *Biomedicines*, 2023, **11**(2), 292.

55 G. Coco, G. Ambrosini, S. Poletti, L. A. Meliante, A. Taloni, V. Scorcia and G. Giannaccare, Recent advances in drug treatments for dry eye disease, *Expet Opin. Pharmacother.*, 2023, **24**(18), 2059–2079.

56 T. Suárez-Cortés, N. Merino-Inda and J. M. Benitez-del-Castillo, Tear and ocular surface disease biomarkers: A diagnostic and clinical perspective for ocular allergies and dry eye disease, *Exp. Eye Res.*, 2022, **221**, 109121.

57 Y. Wu, M. Szymanska, Y. Hu, M. I. Fazal, N. Jiang, A. K. Yetisen and M. F. Cordeiro, Measures of disease activity in glaucoma, *Biosens. Bioelectron.*, 2022, **196**, 113700.

58 T. H. Tsung, Y. C. Tsai, H. P. Lee, Y. H. Chen and D. W. Lu, Biodegradable polymer-based drug-delivery systems for ocular diseases, *Int. J. Mol. Sci.*, 2023, **24**(16), 12976.

59 N. R. Agarwal, M. Tommasini, E. Ciusani, A. Lucotti, S. Trusso and P. M. Ossi, Protein-metal interactions probed by SERS: lysozyme on nanostructured gold surface, *Plasmonics*, 2018, **13**, 2117–2124.

60 S. Zavatski, N. Khinevich, K. Girel, S. Redko, N. Kovalchuk, I. Komissarov, V. Lukashevich, I. Semak, K. Mamatkulov, M. Vorobyeva and G. Arzumanyan, Surface enhanced

Raman spectroscopy of lactoferrin adsorbed on silvered porous silicon covered with graphene, *Biosensors*, 2019, **9**(1), 34.

61 C. Camerlingo, M. Lisitskiy, M. Lepore, M. Portaccio, D. Montorio, S. D. Prete and G. Cennamo, Characterization of human tear fluid by means of surface-enhanced Raman spectroscopy, *Sensors*, 2019, **19**(5), 1177.

62 J. Hu, R. S. Sheng, Z. S. Xu and Y. E. Zeng, Surface enhanced Raman spectroscopy of lysozyme, *Spectrochim. Acta, Part A*, 1995, **51**(6), 1087–1096.

63 G. Cennamo, D. Montorio, V. B. Morra, C. Criscuolo, R. Lanzillo, E. Salvatore, C. Camerlingo, M. Lisitskiy, I. Delfino, M. Portaccio and M. Lepore, Surface-enhanced Raman spectroscopy of tears: toward a diagnostic tool for neurodegenerative disease identification, *J. Biomed. Opt.*, 2020, **25**(8), 087002.

64 P. Hu, X. S. Zheng, C. Zong, M. H. Li, L. Y. Zhang, W. Li and B. Ren, Drop-coating deposition and surface-enhanced Raman spectroscopies (DCDRS and SERS) provide complementary information of whole human tears, *J. Raman Spectrosc.*, 2014, **45**(7), 565–573.

65 R. Swathi, J. Reena, P. Ajeetkumar, O. Ravikiran, D. Tom, K. VB and C. Santhosh, Optical biopsy and optical pathology: affordable health care under low-resource settings, *J. Biomed. Photonics Eng.*, 2020, **6**(2), 20309.

66 P. T. Freire, F. M. Barboza, J. A. Lima, F. E. Melo, J. Mendes Filho, in. *Raman spectroscopy of amino acid crystal, Raman Spectroscopy and Applications*, 2017, vol. 201, p. 171.

67 S. Choi, S. W. Moon, J. H. Shin, H. K. Park and K. H. Jin, Label-free biochemical analytic method for the early detection of adenoviral conjunctivitis using human tear biofluids, *Anal. Chem.*, 2014, **86**(22), 11093–11099.

68 J. Filik, N. Stone, Raman point mapping of tear ferning patterns, in. *Biomedical Optical Spectroscopy*, SPIE, 2008, vol. 6853, pp. 70–75.

69 V. Kopecký Jr and V. Baumruk, Structure of the ring in drop coating deposited proteins and its implication for Raman spectroscopy of biomolecules, *Vib. Spectrosc.*, 2006, **42**(2), 184–187.

70 M. P. Mcoyi, K. T. Mpofu, M. Sekhwama and P. Mthunzi-Kufa, Developments in localized surface plasmon resonance, *Plasmonics*, 2024, 1–40.

71 M. E. Khosroshahi, R. Chabok, N. Chung and Y. Patel, Optimization of immersion direction and time of covalently self-assembled monolayer gold nanourchins on glass as SERS substrate, *J. Nanoparticle Res.*, 2023, **25**(5), 97.

72 R. V. John, T. Devasia, S. S. Adigal, J. Lukose, V. B. Kartha and S. Chidangil, Serum protein profile study of myocardial infarction using a LED induced fluorescence based HPLC system, *J. Chromatogr. B*, 2023, **1217**, 123616.